Inorg. Chem. **2008**, *47*, 4329−4337

Theoretical Study of Pyrazolate-Bridged Dinuclear Platinum(II) Complexes: Interesting Potential Energy Curve of the Lowest Energy Triplet Excited State and Phosphorescence Spectra

Ken Saito,[†] Yoshihide Nakao,[†] and Shigeyoshi Sakaki*[,†,‡]

Department of Molecular Engineering, Graduate School of Engineering, Kyoto University, Nishikyo-ku, Kyoto 615-8510, Japan, and Fukui Institute for Fundamental Chemistry, Kyoto University, Nishihiraki-chou, Takano, Sakyo-ku, Kyoto 606-8103, Japan

Received December 5, 2007

Four kinds of 3,5-dialkylpyrazolate(R_2pz)-bridged dinuclear platinum(II) complexes $[Pt_2(\mu\text{-}R_2pz)_2(dfppy)_2]$ (dfppy = 2-(2,4-difluorophenyl)pyridine; R_2pz = pyrazolate in **1**, 3,5-dimethylpyrazolate in **2**, 3-methyl-5-*tert*-butylpyrazolate in **3**, and 3,5-bis(*tert*-butyl)pyrazolate in **4**) were theoretically investigated by the DFT(B3PW91) method. The Stokes shift of their phosphorescence spectra was discussed on the basis of the potential energy curve (PEC) of the lowest energy triplet excited state (T_1). This PEC significantly depends on the bulkiness of substituents on pz. In **1** and **2**, bearing small substituents on pz, one local minimum is present in the T_1 state besides a global minimum. The local minimum geometry is similar to the S_0-equilibrium one. The T_1 state at this local minimum is characterized as the π-π^* excited state in dfppy, where the dπ orbital of Pt participates in this excited state through an antibonding interaction with the π orbital of dfppy; in other words, this triplet excited state is assigned as the mixture of the ligand-centered π-π^* excited and metal-to-ligand charge transfer excited state (^{3}LC/MLCT). The geometry of the T_1-global minimum is considerably different from the S_0-equilibrium one. The T_1 state at the global minimum is characterized as the triplet metal−metal-to-ligand charge transfer (^{3}MMLCT) excited state, which is formed by the one-electron excitation from the dσ-dσ antibonding orbital to the π^* orbital of dfppy. Because of the presence of the local minimum, the geometry change in the T_1 state is suppressed in polystyrene at room temperature (RT) and frozen 2-methyltetrahydrofuran (2-MeTHF) at 77 K. As a result, the energy of phosphorescence is almost the same in these solvents. In fluid 2-MeTHF at RT, on the other hand, the geometry of the T_1 state easily reaches the T_1-global minimum. Because the T_1-global minimum geometry is considerably different from the S_0-equilibrium one, the phosphorescence occurs at considerably low energy. These are the reasons why the Stokes shift is very large in fluid 2-MeTHF but small in polystyrene and frozen 2-MeTHF. In **3** and **4**, bearing bulky *tert*-butyl substituents on pz, only the T_1-global minimum is present but the local minimum is not. The electronic structure of this T_1-global minimum is assigned as the ^{3}MMLCT excited state like **1** and **2**. Though frozen 2-MeTHF suppresses the geometry change of **3** and **4** in the T_1 state, their geometries moderately change in polystyrene because of the absence of the T_1-local minimum. As a result, the energy of phosphorescence is moderately lower in polystyrene than in frozen 2-MeTHF. The T_1-global minimum geometry is much different from the S_0-equilibrium one in **3** but moderately different in **4**, which is interpreted in terms of the symmetries of these complexes and the steric repulsion between the *tert*-butyl group on pz and dfppy. Thus, the energy of phosphorescence of **3** is much lower in fluid 2-MeTHF than in frozen 2-MeTHF like **1** and **2** but that of **4** is moderately lower; in other words, the Stokes shift in fluid 2-MeTHF is small only in **4**.

1. Introduction

Luminescence spectra of transition metal complexes have been investigated well so far in both fundamental chemistry and applied chemistry because luminescence spectra provide valuable knowledge of the excited state and also emissive compounds are useful as optical materials such as light-emitting devices, photochemical sensors, and biological labeling probes.[1–3] In particular, the 5d transition metal complexes such as iridium[2] and platinum complexes[2a,3–6] have drawn considerable interest because most of them exhibit strong phosphorescence spectra.

* To whom correspondence should be addressed. E-mail: sakaki@moleng.kyoto-u.ac.jp. Fax: +81-75-383-2799.
† Department of Molecular Engineering.
‡ Fukui Institute for Fundamental Chemistry.

10.1021/ic702367f CCC: $40.75
Published on Web 04/17/2008

Scheme 1

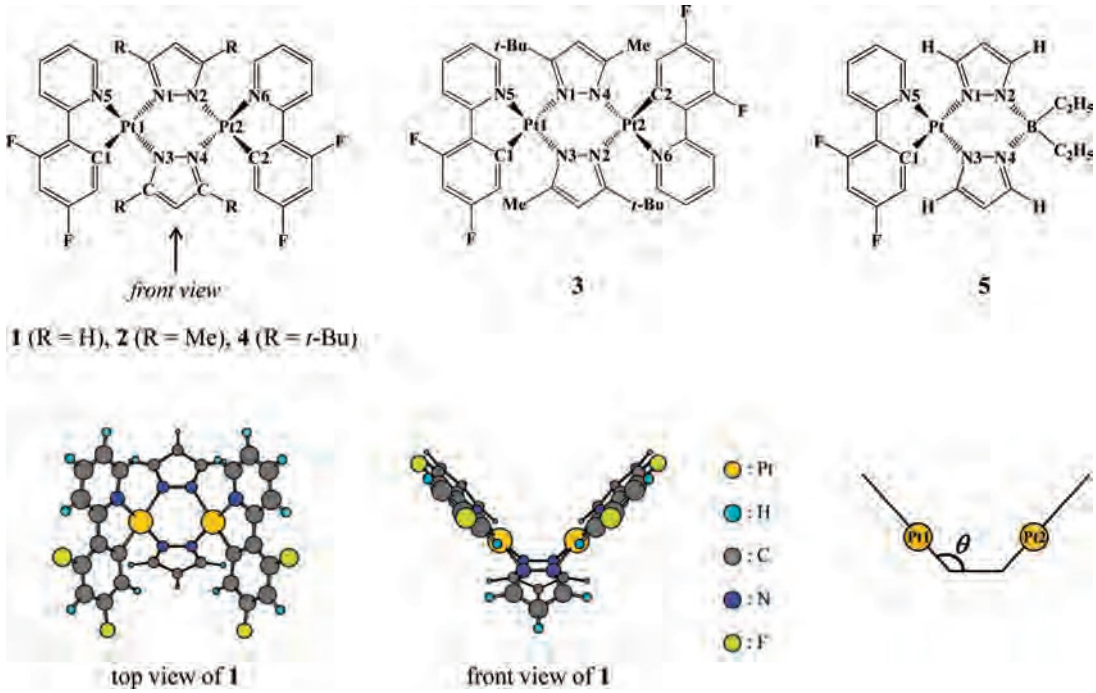

Recently, new characteristic phosphorescence spectra were reported in multinuclear platinum complexes.[1c,2a,3–5] Interestingly, those spectra are much different from those of mononuclear complexes. For instance, phosphorescence spectra of pyrazolate-bridged dinuclear platinum(II) complexes, $[Pt_2(\mu\text{-}R_2pz)_2(dfppy)_2]$ (dfppy = 2-(2,4-difluorophenyl)pyridine; R_2pz = pyrazolate in **1**, 3,5-dimethylpyrazolate in **2**, 3-methyl-5-*tert*-butylpyrazolate in **3**, and 3,5-bis(*tert*-butyl)pyrazolate in **4**; Scheme 1), which were reported by Thompson and his collaborators,[5] are interesting for the reasons that follow: (1) The energies of phosphorescence of **1** and **2** are almost the same in both polystyrene at room temperature (RT) and 2-methyltetrahydrofuran (2-MeTHF) at 77 K, while the energies of phosphorescence of **3** and **4** are moderately lower in the former solution than in the latter one. (2) The energy of phosphorescence of **3** is much lower in fluid 2-MeTHF at RT than in frozen 2-MeTHF at 77 K, while the energy of phosphorescence of **4** is moderately lower in the former solution than in the latter one. These interesting features were discussed in terms of the geometries and the electronic structures of the singlet ground state (S_0) and the lowest energy triplet excited state (T_1).[5] Thus, it is worth theoretically investigating the geometries and the electronic structures of the ground and excited states of these complexes.

In this study, we theoretically investigated the pz-bridged dinuclear platinum(II) complexes, **1**−**4**. Our purposes here are to present theoretical knowledge of the geometries, the electronic structures, and the potential energy curves (PECs) of the S_0 and T_1 states of these complexes and to clarify the reason why their phosphorescence spectra depend considerably on the substituents on pz and the measurement conditions.

2. Computational Details

We employed two basis set systems (basis-I and -II) in this study. In basis-I, core electrons (up to 4f) of Pt were replaced with the relativistic effective core potentials (ECPs) proposed by Hay and Wadt,[7] and its valence electrons were represented by a (541/541/111/1) basis set.[8,9] The 6-31G* basis sets[10] were used for H, C, N, and F. In basis-II, valence electrons of Pt were represented by a (5311/5311/111/1) basis set[8,9] with the same ECPs as those of basis-I. The cc-pVDZ basis sets[11] were used for H, C, N, and F.

(1) Selected reviews for emissive complexes applied to optical meterials: (a) Amendola, V.; Fabbrizzi, L.; Foti, F.; Licchelli, M.; Mangano, C.; Pallavicini, P.; Poggi, A.; Sacchi, D.; Taglietti, A. *Coord. Chem. Rev.* **2006**, *250*, 273. (b) Rogers, C. W.; Wolf, M. O. *Coord. Chem. Rev.* **2002**, *233*−*234*, 341. (c) Keefe, M. H.; Benkstein, K. D.; Hupp, J. T. *Coord. Chem. Rev.* **2000**, *205*, 201.

(2) Selected reviews for emissive iridium complexes applied to optical materials: (a) Evans, R. C.; Douglas, P.; Winscom, C. J. *Coord. Chem. Rev.* **2006**, *250*, 2093. (b) Marin, V.; Holder, E.; Hoogenboom, R.; Schubert, U. S. *Chem. Soc. Rev.* **2007**, *36*, 618. (c) Lo, K. K.-W.; Hui, W.-K.; Chung, C.-K.; Tsang, K. H.-K.; Lee, T. K.-M.; Li, C.-K.; Lau, J. S.-Y.; Ng, D. C.-M. *Coord. Chem. Rev.* **2006**, *250*, 1724. (d) Lo, K. K.-W.; Hui, W.-K.; Chung, C.-K.; Tsang, K. H.-K.; Ng, D. C.-M.; Zhu, N.; Cheung, K.-K. *Coord. Chem. Rev.* **2005**, *249*, 1434.

(3) Selected reviews for emissive platinum complexes applied to optical meterials: (a) Yam, V. W.-W. *Acc. Chem. Res.* **2002**, *35*, 555. (b) Hissler, M.; McGarrah, J. E.; Connick, W. B.; Geiger, D. K.; Cummings, S. D.; Eisenberg, R. *Coord. Chem. Rev.* **2000**, *208*, 115. (c) Paw, W.; Cummings, S. D.; Mansour, M. A.; Connick, W. B.; Geiger, D. K.; Eisenberg, R. *Coord. Chem. Rev.* **1998**, *171*, 125.

(4) Selected review for fundamental study of emissive platinum complexes: (a) Wong, K. M.-C.; Hui, C.-K.; Yu, K.-L.; Yam, V. W.-W. *Coord. Chem. Rev.* **2002**, *229*, 123.

(5) Ma, B.; Li, J.; Djurovich, P. I.; Yousufuddin, M.; Bau, R.; Thompson, M. E. *J. Am. Chem. Soc.* **2005**, *127*, 28.

(6) Brooks, J.; Babayan, Y.; Lamansky, S.; Djurovich, P. I.; Tsyba, I.; Bau, R.; Thompson, M. E. *Inorg. Chem.* **2002**, *41*, 3055.

(7) Hay, P. J.; Wadt, W. R. *J. Chem. Phys.* **1985**, *82*, 299.

(8) Couty, M.; Hall, M. B. *J. Comput. Chem.* **1996**, *17*, 1359.

(9) Ehlers, A. W.; Böhme, M.; Dapprich, S.; Gobbi, A.; Höllwarth, A.; Jonas, V.; Köhler, K. F.; Stegmann, R.; Veldkamp, A.; Frenking, G. *Chem. Phys. Lett.* **1993**, *208*, 111.

(10) (a) Hehre, W. J.; Ditchfield, R.; Pople, J. A. *J. Chem. Phys.* **1972**, *56*, 2257. (b) Hariharan, P. C.; Pople, J. A. *Theor. Chim. Acta* **1973**, *28*, 213.

(11) Dunning, T. H. *J. Chem. Phys.* **1989**, *90*, 1007.

Table 1. Several Important Optimized Bond Lengths (Å), Bond Angles (deg), Dihedral Angles (deg),[a] and Energies of π^*(dfppy), dσ^*(Pt−Pt), and π(dfppy) Orbitals (eV)[b] of **1**−**5**

	1				**2**			
	expt[c]	**1S$_0$**	**1T$_{1a}$**	**1T$_{1b}$**	expt[c]	**2S$_0$**	**2T$_{1a}$**	**2T$_{1b}$**
r(Pt1−Pt2)	3.376	3.395	2.735	3.410	3.191	3.239	2.724	3.252
r(Pt1−N1)	2.082	2.117	2.140	2.119	2.057	2.124	2.138	2.124Z
r(Pt1−N3)	2.009	1.988	2.032	2.027	2.020	2.017	2.030	2.018
r(Pt1−N5)	2.013	2.027	2.010	1.996	2.007	2.028	2.014	2.027
r(Pt1−C1)	1.996	1.988	1.989	1.962	2.001	1.987	1.990	1.987
a(N1−Pt1−N3)	85.5	85.1	85.0	85.1	86.4	84.6	85.1	84.6
a(N5−Pt1−C1)	81.5	81.1	81.6	82.4	80.8	81.0	81.5	81.0
d(Pt1−N1−N3-N4)[d]	132.6	132.3	116.9	132.6	128.3	128.0	116.6	128.4
$\varepsilon(\pi^*$(dfppy))		−2.04	−2.25	−2.24		−1.99	−2.18	−2.18
ε(dσ^*(Pt−Pt))[e]		−5.85	−4.96	−5.93		−5.60	−4.85	−5.65
$\varepsilon(\pi$(dfppy))		−6.50	−6.23	−6.51		−6.45	−6.59	−6.52

	3			**4**			**5**		
	expt[c]	**3S$_0$**	**3T$_{1a}$**	expt[c]	**4S$_0$**	**4T$_{1a}$**	expt[c]	**5S$_0$**	**5T$_1$**
r(Pt1−Pt2)	3.046	3.044	2.686	2.834	2.939	2.649			
r(Pt1−N1)	2.096	2.155	2.167	2.121	2.161	2.166	2.074	2.118	2.118
r(Pt1−N3)	2.031	2.020	2.027	2.054	2.043	2.052	2.010	2.020	2.029
r(Pt1−N5)	2.004	2.031	2.023	2.015	2.029	2.017	2.006	2.028	1.998
r(Pt1−C1)	1.979	1.984	1.986	1.987	1.985	1.995	1.981	2.020	1.968
a(N1−Pt1−N3)	85.2	84.8	85.2	86.0	85.9	86.4	84.7	84.3	84.7
a(N5−Pt1−C1)	81.2	80.9	81.3	81.1	80.9	81.3	80.6	80.7	81.9
d(Pt1−N1−N3-N2)[d]	130.3	128.2	120.7						
d(Pt1−N1−N3-N4)[d]				118.4	120.7	114.8	140.9	144.8	145.9
$\varepsilon(\pi^*$(dfppy))		−2.00	−2.16		−2.04	−2.25		−2.12	−2.37
ε(dσ^*(Pt−Pt))[e]		−5.38	−4.81		−5.07	−4.58			
$\varepsilon(\pi$(dfppy))		−6.49	−6.48		−6.49	−6.34		−6.14	−5.99

[a] The geometries were optimized with the DFT(B3PW91)/basis-I method. [b] The orbital energies were calculated in the S_0 state with the DFT(B3PW91)/basis-II method, where the S_0-, T_{1a}-, and T_{1b}-optimized geometries were employed for the S_0, T_{1a}, and T_{1b} states, respectively. [c] See ref 5. These are the averaged values for C_s symmetry in **1**, **2**, and **4** and C_2 symmetry in **3**. For instance, *r*(Pt1−N1) in this table corresponds to the average value of *r*(Pt1−N1) and *r*(Pt2−N2) reported experimentally. [d] The dihedral angle corresponds to θ in Scheme 1. [e] This represents the HOMO of the S_0 state.

The geometries of **1**−**5** were optimized by the DFT(B3PW91)/basis-I method[12,13] in both the S_0 and the T_1 states. We ascertained that each optimized geometry exhibited no imaginary frequency. The PECs of **1**−**4** were evaluated as a function of the Pt−Pt distance in the S_0 and T_1 states, where all geometrical parameters were optimized with the DFT(B3PW91)/basis-I method at each Pt−Pt distance. The energy of phosphorescence was defined as the energy difference between the S_0 and the T_1 states at either the T_1-global or the T_1-local minimum geometry. This energy difference was calculated by the DFT(B3PW91)/basis-II method.

The solvent effect of fluid 2-MeTHF was taken into consideration by the polarized continuum model (PCM),[14] where THF was employed as a model of 2-MeTHF as in previous theoretical study.[15]

All calculations were performed with the Gaussian 03 (revision C.02) program package.[16] Molecular orbitals were drawn by the MOLEKEL (version 4.3) program.[17]

3. Results and Discussion

3.1. Geometry and Electronic Structure of the S_0 State. The optimized geometries of **1**−**4** in the S_0 state are named **1S$_0$**−**4S$_0$**, respectively, hereafter. As shown in Table 1 and Figure 1, the optimized geometrical parameters including the Pt−Pt distance of **1S$_0$**, **2S$_0$**, and **3S$_0$** agree well with those of the experimental ones, while the optimized Pt−Pt distance of **4S$_0$** is moderately longer than that of the experimental one. The geometry of the Pt−dfppy moiety is almost the same in **1S$_0$**−**4S$_0$** (see Table 1 for the Pt1−N5 length, the N5−Pt1−C1 angle, etc.). Interestingly, the Pt−Pt distance becomes shorter in the order **1** > **2** > **3** > **4**, and the θ angle between the Pt−dfppy moiety and the N1−N2−

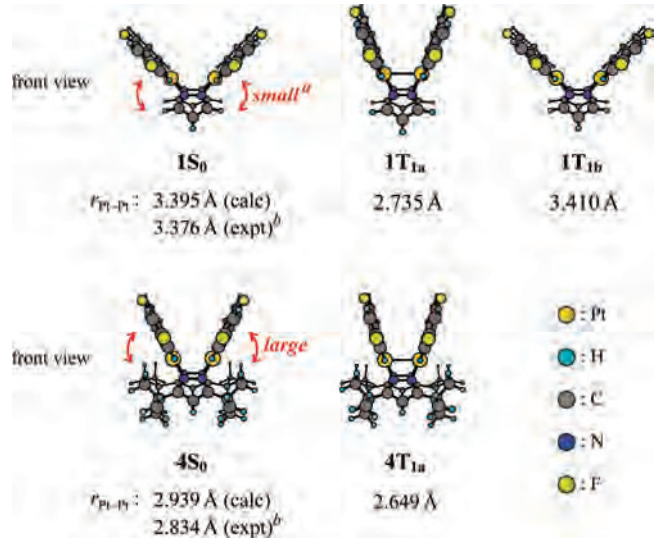

Figure 1. S_0- and T_1-optimized geometries of **1** and **4**. (a) Red arrow schematically represents the steric repulsion between dfppy and the substituents (H atoms in **1** and *tert*-butyl groups in **4**) on pz. (b) See ref 5.

(12) Becke, A. D. *J. Chem. Phys.* **1993**, *98*, 5648.
(13) Perdew, J. P.; Wang, Y. *Phys. Rev. B* **1992**, *45*, 13244.
(14) (a) Mennucci, B.; Tomasi, J. *J. Chem. Phys.* **1997**, *106*, 5151. (b) Cancès, M. T.; Mennucci, B.; Tomasi, J. *J. Chem. Phys.* **1997**, *107*, 3032. (c) Cossi, M.; Barone, V.; Mennucci, B.; Tomasi, J. *Chem. Phys. Lett.* **1998**, *286*, 253. (d) Tomasi, J.; Persico, M. *Chem. Rev.* **1994**, *94*, 2027.
(15) Jakowski, J; Simons, J. *J. Am. Chem. Soc.* **2003**, *125*, 16089.
(16) Pople, J. A.; et al. *Gaussian 03*, Revision C.02; Gaussian, Inc.: Wallingford, CT, 2004.
(17) (a) Flükiger, P.; Lüthi, H. P.; Portmann, S.; Weber, J. *MOLEKEL*, Version 4.3; Scientific Computing: Manno, Switzerland, 2000. (b) Portmann, S.; Lüthi, H. P. *Chimia* **2000**, *54*, 766.

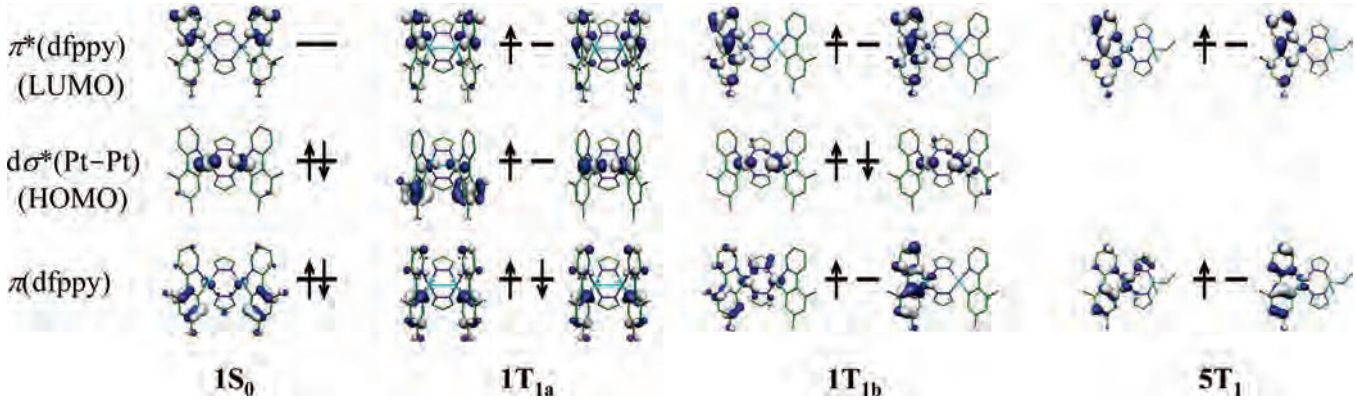

Figure 2. Several important molecular orbitals of $\mathbf{1S_0}$, $\mathbf{1T_{1a}}$, $\mathbf{1T_{1b}}$, and $\mathbf{5T_1}$. H atoms are omitted for brevity.

N3−N4 plane decreases in the same order in both the experimental and the calculated geometries, where the N1, N2, N3, and N4 are on one plane[18] and the θ angle is defined in Scheme 1. These experimental results are explained in terms of the steric repulsion between dfppy and the substituents on pz, as follows: In $\mathbf{1S_0}$, the H atoms on pz slightly push the dfppy plane away, leading to the large θ angle and the long Pt−Pt distance, as shown in Figure 1. In $\mathbf{2S_0}$, the four methyl groups on pz moderately push the dfppy plane away to moderately decrease the Pt−Pt distance and the θ angle (see Figure S1 of the Supporting Information). In $\mathbf{3S_0}$, the two methyl and two *tert*-butyl groups considerably push the dfppy plane away to considerably decrease the Pt−Pt distance and the θ angle. In $\mathbf{4S_0}$, the four *tert*-butyl groups on pz strongly push the dfppy plane away to greatly decrease the Pt−Pt distance and the θ angle.

The highest occupied molecular orbitals (HOMOs) of $\mathbf{1S_0}$−$\mathbf{4S_0}$ mainly consist of the dσ-dσ antibonding overlap between two Pt nuclei, and their lowest unoccupied molecular orbitals (LUMOs) mainly consist of the π^* orbital of dfppy, as shown in Figure 2. The HOMO is named the dσ^*(Pt−Pt) orbital hereafter because the dσ orbital of one Pt atom overlaps with the dσ orbital of the other Pt atom in an antibonding way. The π orbital of dfppy is at moderately lower energy than the HOMO. As the Pt−Pt distance becomes shorter, the dσ-dσ antibonding overlap increases. As a result, the dσ^*(Pt−Pt) orbital energy becomes higher with a decrease in the Pt−Pt distance, as clearly shown in Figure 3, in which the dσ^*(Pt−Pt) orbital energies are plotted against the Pt−Pt distance. On the other hand, the π and π^* orbital energies of dfppy (Figure 2) slightly depend on the Pt−Pt distance, as expected. In addition, these orbital energies are almost the same as those of the mononuclear Pt(II) complex [Pt(μ-pz)$_2$(dfppy)B(C_2H_5)$_2$] (**5**), as shown in Table 1.

These features observed in the S_0 geometry, the HOMO, and the LUMO deeply relate to the phosphorescence spectra of those complexes, as will be discussed below.

(18) Because the dihedral angle d(N1−N2−N3−N4) is 180.0° in $\mathbf{1S_0}$, $\mathbf{2S_0}$, and $\mathbf{4S_0}$, the N1, N2, N3, and N4 are in one plane. In $\mathbf{3S_0}$, the dihedral angle d(N1−N4−N3−N2) is 168.4°, indicating that these atoms are not on one plane, strictly speaking. However, the deviation from the plane is small.

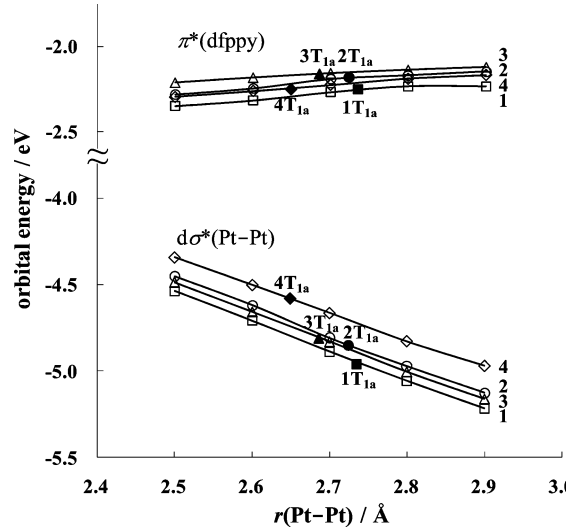

Figure 3. Energies of the dσ^*(Pt−Pt) orbital (HOMO of the S_0 state) and the π^*(dfppy) orbital (LUMO of the S_0 state) of **1**−**4** vs the Pt−Pt distance. These orbital energies were calculated in the S_0 state with the DFT(B3PW91)/basis-II method. The geometries were optimized in the T_1 state at each Pt−Pt distance with the DFT(B3PW91)/basis-I method.

3.2. Geometry and Electronic Structure of the T_1 State. There are two possible lowest energy triplet excited states, as shown in Figure 2. In one ($\mathbf{1T_{1a}}$), one-electron excitation occurs from the dσ^*(Pt−Pt) orbital to the π^* orbital of dfppy. In the other ($\mathbf{1T_{1b}}$), one-electron excitation occurs from the π orbital to the π^* orbital in dfppy. The former is named metal−metal-to-ligand charge transfer (MMLCT) excitation and the latter is the π-π^* excitation. First, we optimized the geometry of the former excited state, which corresponds to the T_1-global minimum ($\mathbf{1T_{1a}}$−$\mathbf{4T_{1a}}$), as will be shown below. Its optimized geometrical parameters are presented in Table 1 and Figure 1 (see also Figure S1 of the Supporting Information for the T_1-global minimum geometries of **2** and **3**). The Pt−Pt distance is much shorter and the θ angle is much smaller in all the T_1-global minimum geometries ($\mathbf{1T_{1a}}$−$\mathbf{4T_{1a}}$) than in all the S_0-equilibrium ones ($\mathbf{1S_0}$−$\mathbf{4S_0}$). This result is explained in terms of the dσ-dσ bonding interaction, as follows: In $\mathbf{1S_0}$, this bonding interaction is not formed at all because the antibonding dσ^*(Pt−Pt) orbital is doubly occupied, as shown in Figure 2. In $\mathbf{1T_{1a}}$, on the other hand, one-electron excitation occurs from the dσ^*(Pt−Pt) orbital to the π^* orbital of dfppy. As a result,

the dσ*(Pt−Pt) orbital becomes singly occupied, which leads to the formation of the Pt−Pt bonding interaction and the decrease of the Pt−Pt distance in $\mathbf{1T_{1a}}$. The difference (0.086 Å) in the Pt−Pt distance between $\mathbf{1T_{1a}}$ and $\mathbf{4T_{1a}}$ is much smaller than that (0.456 Å) between $\mathbf{1S_0}$ and $\mathbf{4S_0}$. This result indicates that the T_1-global minimum geometry depends less on the substituents on pz than does the S_0-equilibrium one. This is because the Pt−Pt bonding interaction in addition to the substituents on pz plays important roles to determine the Pt−Pt distance of the T_1-global minimum but only the substituents on pz play important roles to determine the Pt−Pt distance in the S_0 state. Thus, the Pt−Pt distance depends less on the substituent on pz in the T_1-global minimum than in the S_0 state.

The dσ*(Pt−Pt) orbital is at a much higher energy in the T_1-global minimum geometry than in the S_0-equilibrium one in all complexes, as shown in Table 1. This is because the Pt−Pt distance is much shorter in the T_1-global minimum geometry than in the S_0-equilibrium one; note that the dσ*(Pt−Pt) orbital energy becomes higher as the Pt−Pt distance becomes shorter (Figure 2) because this orbital involves the dσ-dσ antibonding overlap. It is noted that the orbital energy of $\mathbf{4T_{1a}}$ is the highest in all the T_1-global minima, as shown in Table 1 and Figure 3. This is because the Pt−Pt distance of $\mathbf{4T_{1a}}$ is the shortest in these T_1-global minima. On the other hand, the dσ*(Pt−Pt) orbital is at a much lower energy in $\mathbf{1T_{1a}}$ and $\mathbf{2T_{1a}}$ because the Pt−Pt distance is considerably longer in these geometries. It is also noted that the orbital energy of $\mathbf{3T_{1a}}$ is little different from those of $\mathbf{1T_{1a}}$ and $\mathbf{2T_{1a}}$ (see Figure 3) in spite of the shorter Pt−Pt distance of $\mathbf{3T_{1a}}$ than those of $\mathbf{1T_{1a}}$ and $\mathbf{2T_{1a}}$, as clearly shown in Table 1. These results are interpreted in terms of the symmetries of these complexes. Because all substituents on pz are the same in **1**, **2**, and **4** (H atoms in **1**, methyl groups in **2**, and *tert*-butyl groups in **4**; see Schemes 1 and 2), both the phenyl and the pyridine moieties of dfppy are pushed away to a similar extent by these substituents on pz. As a result, $\mathbf{1T_{1a}}$, $\mathbf{2T_{1a}}$, and $\mathbf{4T_{1a}}$ take the C_s-like geometry. Because the d_{z^2} orbital of Pt1 expands toward the Pt2 atom in this geometry, the dσ-dσ antibonding overlap is large, which considerably raises the dσ*(Pt−Pt) orbital energy. In **3**, two large *tert*-butyl groups and two small methyl groups are introduced to pz. Because the pyridine moiety of dfppy is strongly pushed away by the *tert*-butyl group but the phenyl moiety is moderately pushed away by the methyl group, as shown in Scheme 2, $\mathbf{3T_{1a}}$ takes not the C_s-like symmetry but the C_2-like one. In this geometry, the d_{z^2} orbital of Pt1 does not expand toward Pt2, and its direction deviates from the Pt−Pt line, which decreases the dσ-dσ antibonding overlap. As a result, the dσ*(Pt−Pt) orbital energy of **3** is not destabilized very much but becomes similar to those of **1** and **2** in spite of its shorter Pt−Pt distance than those of **1** and **2**.

We tried to optimize the T_1-geometry with the π-π* excitation of dfppy and found a T_1-local minimum of **1** and **2** ($\mathbf{1T_{1b}}$ and $\mathbf{2T_{1b}}$), as shown in Table 1 and Figure 1. We ascertained that these local minima have no imaginary frequency. These T_1-local minima are less stable than the

Scheme 2[a]

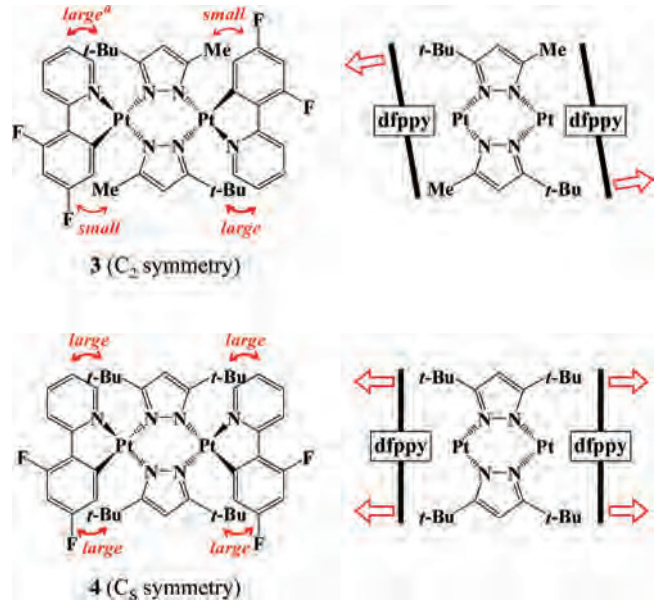

[a] Red arrows schematically represent the steric repulsion between dfppy and the substituents on pz.

T_1-global minima by 0.09 eV in **1** and 0.21 eV in **2**.[19] Their geometries are similar to the S_0-equilibrium geometries unlike $\mathbf{1T_{1a}}$ and $\mathbf{2T_{1a}}$. This is easily understood in terms of the electronic structures of $\mathbf{1T_{1b}}$ and $\mathbf{2T_{1b}}$. Because the dσ*(Pt−Pt) orbital is doubly occupied in $\mathbf{1T_{1b}}$ and $\mathbf{2T_{1b}}$ like $\mathbf{1S_0}$ and $\mathbf{2S_0}$, as shown in Figure 2, the dσ-dσ bonding interaction is not formed at all in $\mathbf{1T_{1b}}$ and $\mathbf{2T_{1b}}$, which is consistent with the long Pt−Pt distance of $\mathbf{1T_{1b}}$ (3.410 Å) and $\mathbf{2T_{1b}}$ (3.252 Å). Several interesting features are observed in $\mathbf{1T_{1b}}$ and $\mathbf{2T_{1b}}$, as follows: (1) Though the π and π* orbitals of dfppy are delocalized on the whole molecule in $\mathbf{1S_0}$, $\mathbf{2S_0}$, $\mathbf{1T_{1a}}$, and $\mathbf{2T_{1a}}$, they are localized on one dfppy in $\mathbf{1T_{1b}}$ and $\mathbf{2T_{1b}}$. (2) The dπ(Pt−Pt) orbital weakly interacts with the π orbital of dfppy in an antibonding way in $\mathbf{1S_0}$, $\mathbf{2S_0}$, $\mathbf{1T_{1b}}$, and $\mathbf{2T_{1b}}$, where the dπ(Pt−Pt) represents the dπ-dπ bonding orbital between two Pt atoms. (3) But, the dπ(Pt−Pt) orbital slightly participates with the π* orbital of dfppy in $\mathbf{1T_{1b}}$ and $\mathbf{2T_{1b}}$. Thus, the electronic structures of $\mathbf{1T_{1b}}$ and $\mathbf{2T_{1b}}$ are not simple ligand-centered π-π* excited states but the mixture of ligand-centered π-π* excited states and metal-to-ligand charge transfer excited states (^{3}LC/MLCT). This feature is similar to the T_1 state of **5** ($\mathbf{5T_1}$). Actually, the π(dfppy) and π*(dfppy) orbital energies are almost the same in $\mathbf{1T_{1b}}$, $\mathbf{2T_{1b}}$, and $\mathbf{5T_1}$, as shown in Table 1. In other words, the electronic structures of $\mathbf{1T_{1b}}$ and $\mathbf{2T_{1b}}$ are similar to that of $\mathbf{5T_1}$.

No local minima, which corresponds to $\mathbf{1T_{1b}}$ and $\mathbf{2T_{1b}}$, however, could be optimized in the T_1 state of **3** and **4**. This is easily interpreted in terms of the large steric repulsion between the substituents on pz and dfppy. As shown in Figure 1, this large steric repulsion significantly decreases the Pt−Pt distance even in the ground state; actually, the

(19) These energy differences were calculated with the DFT(B3PW91)/basis-II method, where the T_1-local ($\mathbf{1T_{1b}}$ and $\mathbf{2T_{1b}}$) and T_1-global minimum geometries ($\mathbf{1T_{1a}}$ and $\mathbf{2T_{1a}}$) were optimized with the DFT(B3PW91)/basis-I method.

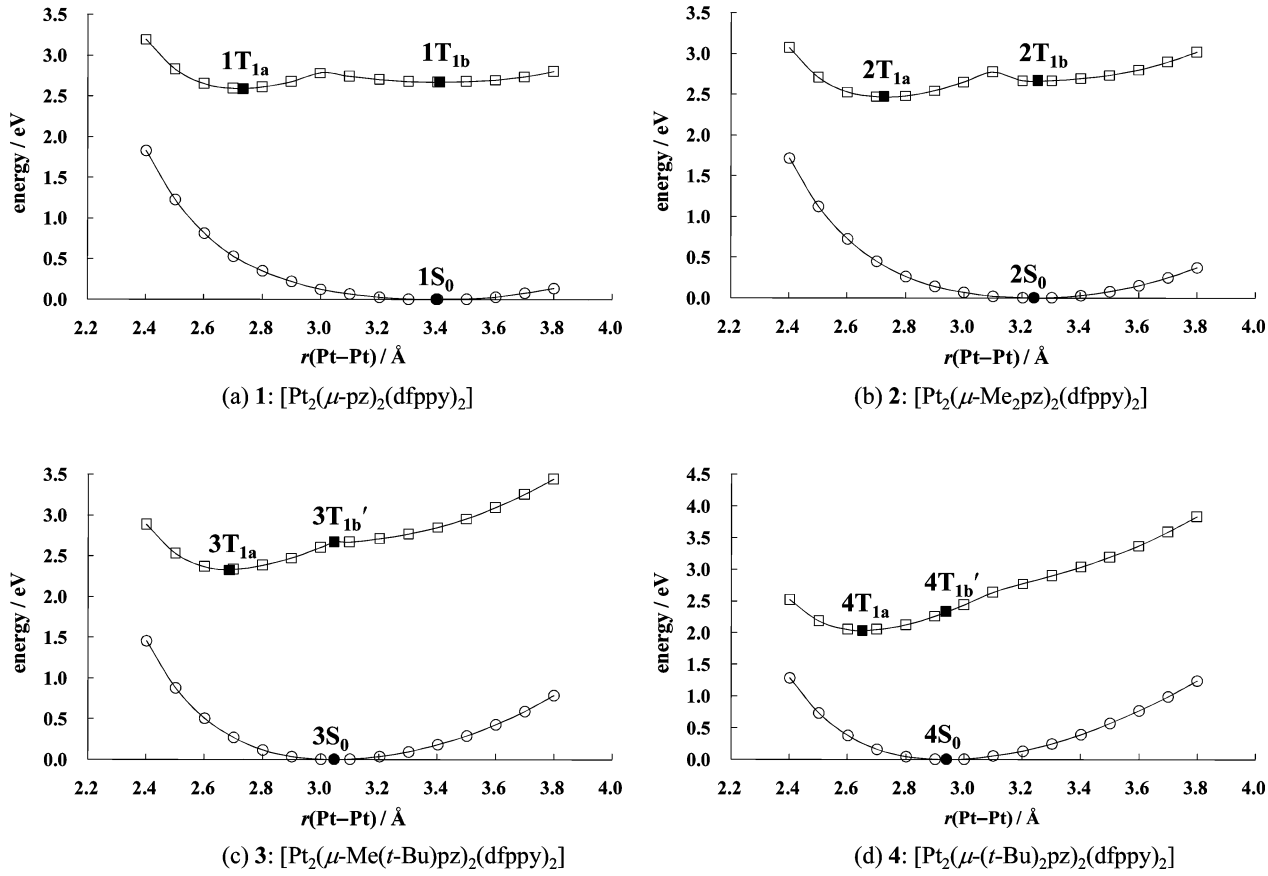

Figure 4. PECs of the S_0 and T_1 states of dinuclear complexes **1**−**4** vs the Pt−Pt distance. The geometries of the S_0 and T_1 states were optimized with the DFT(B3PW91)/basis-I method at each Pt−Pt distance. It is noted that the energy difference between two curves does not correspond to the energy of phosphorescence because the T_1-curve represents the energy of the T_1-optimized geometry and the S_0-curve represents the energy of the S_0-optimized geometry.

Pt−Pt distance of **4** is much shorter than that of **1**. The short Pt−Pt distance considerably destabilizes the dσ*(Pt−Pt) orbital energy, which leads to a considerably stable ^{3}MMLCT excited state relative to the ^{3}LC/MLCT excited state. As a result, the ^{3}LC/MLCT excited state cannot become local minima in **3** and **4**.

3.3. Phosphorescence Spectra of 1 and 2. PECs of the S_0 and T_1 states of **1** and **2** are represented as a function of the Pt−Pt distance (Figure 4a,b), in which both S_0- and T_1-geometries were optimized at each Pt−Pt distance. A small but non-negligible activation barrier exists between the T_1-global (**1T$_{1a}$** and **2T$_{1a}$**) and the T_1-local minima (**1T$_{1b}$** and **2T$_{1b}$**). Because of the presence of this barrier, it is likely that the T_1-geometries of **1** and **2** stay at these T_1-local minima in frozen 2-MeTHF at 77 K and polystyrene at RT, where geometry changes do not easily occur. Thus, the energy of phosphorescence in these conditions corresponds to the energy difference between the T_1 and the S_0 states at the T_1-local minimum geometry (**1T$_{1b}$** and **2T$_{1b}$**). This energy difference is calculated to be 2.35 eV in both complexes, which agrees well with the experimental value,[5] as shown in Table 2. These phosphorescence spectra are assigned as the π*(dfppy) → π(dfppy) + d(Pt) transition because **1T$_{1b}$** and **2T$_{1b}$** are characterized as the ^{3}LC/MLCT excited state, as discussed above. This is theoretical support to the experimental assignment by Thompson et al.[5] Here, we wish to mention two split peaks experimentally observed in the phosphorescence spectra of **1** and **2**, when the measurement is carried out in frozen 2-MeTHF and polystyrene.[5] These split peaks were discussed in terms of the coupling with the breathing vibration of the aromatic ring of dfppy.[5,6] Because such vibrational coupling is not incorporated by the usual electronic structure calculation, we compare here the calculated energy of the phosphorescence with the averaged value of these two peaks.

In contrast to frozen 2-MeTHF at 77 K and polystyrene at RT, fluid 2-MeTHF at RT does not suppress the geometry change. Because the activation barrier between the local and the global minima is small in the T_1-potential energy curve (T_1-PEC), where the height of this activation barrier is 0.12 eV in **1** and 0.07 eV in **2**,[20] the geometries of **1** and **2** in the T_1 state easily change to their T_1-global minima (**1T$_{1a}$** and

(20) The activation barrier corresponds to the energy difference between the T_1-optimized geometry at r(Pt−Pt) = 3.000 Å and the T_1-local minimum geometry (**1T$_{1b}$**) in **1** and between the T_1-optimized geometry at r(Pt−Pt) = 3.100 Å and the T_1-local minimum geometry (**2T$_{1b}$**) in **2**, where the transition state is at r(Pt−Pt) = 3.000 Å in **1** and at r(Pt−Pt) = 3.100 Å in **2**. These energy differences were calculated with the DFT(B3PW91)/basis-II//DFT(B3PW91)/basis-I method, where the geometries were optimized at each Pt−Pt distance. These activation barriers are a little bit overestimated, as follows: Because the transition state here is a crossing point of two states, the transition state should be calculated with a multireference method. However, the values presented here are not very much different from the correct values because the PEC of the T_1 state is not steep but rather flat in the righthand side of the transition state (see Figure 4).

Table 2. Energies (eV)[a] of Phosphorescence Spectra of **1**−**5** and Their Assignments

			energy of phosphorescence			
			calcd			
complex	geometry	assignment	vacuum	THF	expt[b]	
1	$\mathbf{1T_{1b}}$	π^*(dfppy) → π(dfppy) + d(Pt)	2.35	2.37	2.52, 2.71	(2-MeTHF at 77 K)
					2.50, 2.66	(polystyrene at RT)
	$\mathbf{1T_{1a}}$	π^*(dfppy) → dσ^*(Pt−Pt)	1.97	1.92	1.93	(2-MeTHF at RT)
2	$\mathbf{2T_{1b}}$	π^*(dfppy) → π(dfppy) + d(Pt)	2.35	2.37	2.49, 2.68	(2-MeTHF at 77 K)
					2.46, 2.63	(polystyrene at RT)
	$\mathbf{2T_{1a}}$	π^*(dfppy) → dσ^*(Pt−Pt)	1.92	1.98	1.98	(2-MeTHF at RT)
3	$\mathbf{3T_{1b}}'$	π^*(dfppy) → dσ^*(Pt−Pt)	2.54	2.57	2.49	(2-MeTHF at 77 K)
					2.27	(polystyrene at RT)
	$\mathbf{3T_{1a}}$	π^*(dfppy) → dσ^*(Pt−Pt)	1.88	1.92	1.95	(2-MeTHF at RT)
4	$\mathbf{4T_{1b}}'$	π^*(dfppy) → dσ^*(Pt−Pt)	2.17	2.20	2.18	(2-MeTHF at 77 K)
					1.96	(polystyrene at RT)
	$\mathbf{4T_{1a}}$	π^*(dfppy) → dσ^*(Pt−Pt)	1.59	1.63	1.80	(2-MeTHF at RT)
5	$\mathbf{5T_1}$	π^*(dfppy) → π(dfppy) + d(Pt)	2.35	2.36	2.51, 2.69	(2-MeTHF at 77 K)
					2.49, 2.66	(2-MeTHF at RT)

[a] The energy of phosphorescence is defined as the energy difference between the T_1 and S_0 states at the same geometry (vertical transition energy). This energy difference was calculated by the DFT(B3PW91)/basis-II method. [b] See ref 5.

$\mathbf{2T_{1a}}$) in fluid 2-MeTHF. In this case, the energy of phosphorescence corresponds to the energy difference between the T_1 and the S_0 states at the T_1-global minimum geometry. These are calculated to be 1.92 and 1.98 eV in $\mathbf{1T_{1a}}$ and $\mathbf{2T_{1a}}$, respectively, which agree well with the experimental energies,[5] as shown in Table 2. The calculated energy of phosphorescence is little different between vacuum and THF, as shown in Table 2, indicating that the solvent effect is small in the energy of phosphorescence. The phosphorescence in fluid 2-MeTHF is assigned as the π^*(dfppy) → dσ^*(Pt−Pt) transition because the T_1-global minima ($\mathbf{1T_{1a}}$ and $\mathbf{2T_{1a}}$) are characterized as the ^{3}MMLCT excited states, as experimentally reported by Thompson et al.[5]

It is noted that the energy of phosphorescence is much lower in fluid 2-MeTHF at RT than in frozen 2-MeTHF at 77 K and polystyrene at RT, as shown in Table 2. This is interpreted in terms of the PECs of the S_0 and T_1 states. The S_0 state becomes less stable in energy than does the S_0-equilibrium geometry as the Pt−Pt distance becomes shorter, as shown in Figure 4a,b. Because the Pt−Pt distance in the T_1-global minimum geometry is much shorter than in the T_1-local minimum, which is similar to that in the S_0-equilibrium one, the energy difference between the T_1 and the S_0 states is much smaller at the T_1-global minimum geometry than at the T_1-local minimum one. Thus, the Stokes shift is much larger in fluid 2-MeTHF than in frozen 2-MeTHF and polystyrene.

When the phosphorescence spectrum is measured in fluid 2-MeTHF at RT, **1** exhibits two small peaks at 2.52 and 2.71 eV in addition to one large peak at 1.93 eV.[5] On the other hand, **2** exhibits only one peak at 1.93 eV in fluid 2-MeTHF. This difference between **1** and **2** is easily interpreted in terms of the equilibrium between the T_1-global and T_1-local minima. In **1**, the Gibbs free energy difference ($\Delta\Delta G^0$) between $\mathbf{1T_{1a}}$ and $\mathbf{1T_{1b}}$ at 298 K is very small (0.019 eV),[21] which leads to the equilibrium constant (K) of 0.48 and the somewhat large population (about 30%) of $\mathbf{1T_{1b}}$. As a result, the phosphorescence occurs not only at the T_1-global minimum but also at the T_1-local minimum even in fluid 2-MeTHF. The complex **1** in the global minimum presents one large peak at 1.93 eV, and the complex **1** in the local minimum presents two small peaks at 2.52 and 2.71 eV; remember that the vibration coupling was observed at the local minimum. In **2**, however, the population at the local minimum $\mathbf{2T_{1b}}$ is negligibly small because the $\Delta\Delta G^0$ between $\mathbf{2T_{1a}}$ and $\mathbf{2T_{1b}}$ at 298 K is large (0.13 eV). As a result, only one large peak is observed at low energy in **2**.

Here, we wish to make a comparison of the phosphorescence spectra of **1** and **2** with that of the mononuclear complex **5**. The optimized geometry of the T_1 state ($\mathbf{5T_1}$) is almost the same as the S_0-equilibrium one ($\mathbf{5S_0}$), as shown in Table 1. Thus, the Stokes shift is expected to be small and little different between fluid 2-MeTHF and frozen 2-MeTHF. Actually, the experimentally reported phosphorescence spectrum in frozen 2-MeTHF at 77 K is almost the same as that in fluid 2-MeTHF at RT, as shown in Table 2. The energy differences between the S_0 and the T_1 states at $\mathbf{5T_1}$ are 2.35 and 2.36 eV in a vacuum and in 2-MeTHF, respectively, which agree well with the experimental phosphorescence spectrum,[5] as shown in Table 2. This phosphorescence spectrum is assigned as the π^*(dfppy) → π(dfppy) + d(Pt) transition like those of $\mathbf{1T_{1b}}$ and $\mathbf{2T_{1b}}$. This is because $\mathbf{1T_{1b}}$, $\mathbf{2T_{1b}}$, and $\mathbf{5T_1}$ take the ^{3}LC/MLCT excited state, as shown in Figure 2. It is noted that the energies of phosphorescence of $\mathbf{1T_{1b}}$ and $\mathbf{2T_{1b}}$ are almost the same as that of $\mathbf{5T_1}$, indicating that the phosphorescence occurs in $\mathbf{1T_{1b}}$ and

(21) The $\Delta\Delta G^0$ value is defined as the difference in the Gibbs free energy (ΔG^0) between $\mathbf{1T_{1a}}$ and $\mathbf{1T_{1b}}$. Each ΔG^0 value was evaluated as follows: (1) The energies of $\mathbf{1T_{1a}}$ and $\mathbf{1T_{1b}}$ were calculated with the DFT(B3PW91)/basis-II method. (2) The zero-point energy was evaluated with the DFT(B3PW91)/basis-I method. (3) A thermal correction at 298 K was made with the partition function of the vibration movements, in which the partition function was evaluated by the DFT(B3PW91)/basis-I method.

$\mathbf{2T_{1b}}$ like that of the mononuclear complex **5**; in other words, any character of dinuclear complex does not participate in the phosphorescence of $\mathbf{1T_{1b}}$ and $\mathbf{2T_{1b}}$.

3.4. Phosphorescence Spectra of 3 and 4. PECs of the S_0 and T_1 states of **3** and **4** are represented as a function of the Pt−Pt distance in Figure 4c,d. It is noted here that the T_1-local minimum is absent in these PECs. However, the electronic structure of the T_1 state depends on the Pt−Pt distance like **1** and **2**, as follows: The T_1 state of **3** and **4** is the ^{3}MMLCT excited state when the Pt−Pt distance is shorter than 3.10 Å but is the ^{3}LC/MLCT excited state when the Pt−Pt distance is longer than 3.10 Å. Actually, the PEC of the T_1 state is not smooth around 3.10 Å, suggesting that the electronic structure changes around here.

First, we assumed that the phosphorescence of **3** and **4** occurs at the S_0-equilibrium geometry in frozen 2-MeTHF at 77 K like **1** and **2** because the geometry changes little in these conditions. In this case, the energy of phosphorescence corresponds to the energy difference between the T_1 and the S_0 states at the S_0-equilibrium geometry ($\mathbf{3S_0}$ and $\mathbf{4S_0}$); in other words, we assumed that no geometry change occurs in frozen 2-MeTHF. The calculated energies are 2.67 eV in $\mathbf{3S_0}$ and 2.35 eV in $\mathbf{4S_0}$, which are somewhat larger than the experimental values (2.49 eV in **3** and 2.18 eV in **4**; Table 2).[5] These results suggest that the geometry is not completely fixed in frozen 2-MeTHF. It is likely that the solvent cage little changes in frozen 2-MeTHF but the geometry changes occur in this solvent cage. We assumed that the geometry change in the solvent cage occurs without change of the Pt−Pt distance because the change of the Pt−Pt distance would need the change of the solvation cage. Thus, the geometries of **3** and **4** in the T_1 state were optimized with the Pt−Pt distance fixed to be the same as that of the S_0-equilibrium geometry (3.044 Å in **3** and 2.939 Å in **4**). In such optimized geometries ($\mathbf{3T_{1b}}'$ and $\mathbf{4T_{1b}}'$), the energies of phosphorescence are evaluated to be 2.54 and 2.17 eV in **3** and **4**, respectively, which agree well with the experimental values in frozen 2-MeTHF,[5] as shown in Table 2. These results suggest that the geometry changes moderately occur in the solvent cage of frozen 2-MeTHF. The phosphorescence spectra are assigned as the π^*(dfppy) → dσ^*(Pt−Pt) transition because the T_1 state at these Pt−Pt distances is characterized as the ^{3}MMLCT state, as discussed above. The energy of this phosphorescence is considerably lower in $\mathbf{4T_{1b}}'$ than in $\mathbf{3T_{1b}}'$. This result is interpreted in terms of the Pt−Pt distance as follows: Because the Pt−Pt distance (2.939 Å) of $\mathbf{4T_{1b}}'$ is considerably shorter than that (3.044 Å) of $\mathbf{3T_{1b}}'$, the dσ-dσ antibonding overlap is considerably larger in $\mathbf{4T_{1b}}'$ than in $\mathbf{3T_{1b}}'$, which leads to the higher energy of the dσ^*(Pt−Pt) orbital in $\mathbf{4T_{1b}}'$ (−5.02 eV) than in $\mathbf{3T_{1b}}'$ (−5.36 eV). On the other hand, the energy of the π^*(dfppy) orbital is little different between $\mathbf{4T_{1b}}'$ (−2.16 eV) and $\mathbf{3T_{1b}}'$ (−2.11 eV). Thus, the energy of phosphorescence is lower in **4** than in **3**.

In fluid 2-MeTHF at RT, the phosphorescence occurs at the T_1-global minimum geometry ($\mathbf{3T_{1a}}$ and $\mathbf{4T_{1a}}$) like **1** and **2** because the geometry easily changes to the T_1-global minimum. The energy of phosphorescence is evaluated to be 1.92 and 1.63 eV in **3** and **4**, respectively, as shown in Table 2. The calculated energy of **3** agrees well with the experimental value,[5] while that of **4** is moderately lower than the experimental value. These phosphorescence spectra are assigned as the π^*(dfppy) → dσ^*(Pt−Pt) transition because the T_1-global minimum is characterized as the ^{3}MMLCT excited state. This assignment agrees with the experimental proposal.[5] Interestingly, both experimental and theoretical results indicate that the energy of phosphorescence of **4** is much lower than those of **1**, **2**, and **3** in fluid 2-MeTHF. This result is interpreted in terms of the dσ-dσ antibonding overlap. Because the Pt−Pt distance of $\mathbf{4T_{1a}}$ is the shortest in all the T_1-global minimum geometries, the dσ^*(Pt−Pt) orbital of $\mathbf{4T_{1a}}$ is at the highest energy in those of $\mathbf{1T_{1a}}$−$\mathbf{4T_{1a}}$. As a result, the π^*(dfppy) → dσ^*(Pt−Pt) phosphorescence occurs at the lowest energy in **4**.

It is noted here that the energy of phosphorescence of $\mathbf{3T_{1a}}$ is almost the same as those of $\mathbf{1T_{1a}}$ and $\mathbf{2T_{1a}}$, as shown in Table 2, in spite of the shorter Pt−Pt distance of $\mathbf{3T_{1a}}$ than those of $\mathbf{1T_{1a}}$ and $\mathbf{2T_{1a}}$ (see Table 1). This is because the dσ^*(Pt−Pt) orbital of $\mathbf{3T_{1a}}$ is at an energy similar to those of $\mathbf{1T_{1a}}$ and $\mathbf{2T_{1a}}$ (Figure 3); remember that the dσ^*(Pt−Pt) orbital energy of $\mathbf{3T_{1a}}$ is not destabilized very much in spite of the short Pt−Pt distance because the d_{z^2} orbital of one Pt atom does not extend toward the other Pt atom and its direction deviates from the Pt−Pt line in **3** because of the C_2 symmetry of $\mathbf{3T_{1a}}$ (see above and Scheme 2).

The energy of phosphorescence of **4** is moderately lower in fluid 2-MeTHF at RT than in frozen 2-MeTHF at 77 K, but that of **3** is considerably lower in fluid 2-MeTHF at RT than in frozen 2-MeTHF at 77 K. Because the phosphorescence occurs at the T_1-global minimum geometry ($\mathbf{3T_{1a}}$ and $\mathbf{4T_{1a}}$) in fluid 2-MeTHF but at the geometry ($\mathbf{3T_{1b}}'$ and $\mathbf{4T_{1b}}'$) that is similar to the S_0-equilibrium one in frozen 2-MeTHF, the above-mentioned difference between **3** and **4** arises from the difference in the geometry of the T_1 state between **3** and **4**, as follows: The geometry difference between $\mathbf{4T_{1a}}$ and $\mathbf{4S_0}$ is considerably smaller than that between $\mathbf{3T_{1a}}$ and $\mathbf{3S_0}$; for instance, the Pt−Pt distance of the T_1-global minimum is shorter than that of the S_0-equilibrium one by 0.290 Å in **4** and 0.358 Å in **3**, as shown in Table 1. Because the $\mathbf{3S_0}$ and $\mathbf{4S_0}$ geometries are similar to the $\mathbf{3T_{1b}}'$ and $\mathbf{4T_{1b}}'$ geometries, respectively, as discussed above, the T_1 geometry considerably changes upon going from $\mathbf{3T_{1b}}'$ to $\mathbf{3T_{1a}}$ but moderately upon going from $\mathbf{4T_{1b}}'$ to $\mathbf{4T_{1a}}$. This is the reason why the energy of phosphorescence of **4** is moderately lower in fluid 2-MeTHF than in frozen 2-MeTHF but that of **3** is considerably lower in the former solution than in the latter one.

The reason why the geometry difference between $\mathbf{4T_{1a}}$ and $\mathbf{4S_0}$ is smaller than that between $\mathbf{3T_{1a}}$ and $\mathbf{3S_0}$ is explained in terms of the steric repulsion between the substituents on pz and dfppy. As discussed in Section 3.2, the S_0-equilibrium geometry depends considerably on this steric repulsion; because **4** has four large *tert*-butyl substituents but **3** has two large *tert*-butyl and two small methyl substituents on pz, the steric repulsion is much larger in **4** than in **3**. As a

result, the Pt−Pt distance is considerably shorter in the S_0-equilibrium geometry of **4** than of **3**. On the other hand, the T_1-global minimum geometry depends less on the steric repulsion than does the S_0-equilibrium one because the dσ(Pt−Pt) bonding interaction plays important roles to determine the geometry of the T_1-global minimum in addition to the steric repulsion (see above): actually, the Pt−Pt distance of $\mathbf{4S_0}$ is considerably shorter than that of $\mathbf{3S_0}$ by 0.105 Å, but the Pt−Pt distance of $\mathbf{4T_{1a}}$ is little different from that of $\mathbf{3T_{1a}}$ (see Table 1). In other words, the Pt−Pt distance of $\mathbf{4S_0}$ is already short relative to that of $\mathbf{3S_0}$. Thus, the geometry changes take place less upon going to $\mathbf{4T_{1a}}$ from $\mathbf{4S_0}$ than upon going to $\mathbf{3T_{1a}}$ from $\mathbf{3S_0}$.

The energies of phosphorescence in polystyrene at RT are experimentally reported to be 2.27 and 1.96 eV in **3** and **4**, respectively,[5] which are lower than those in frozen 2-MeTHF at 77 K but higher than those in fluid 2-MeTHF at RT, as shown in Table 2. These results are different from those of **1** and **2**, where the energy of phosphorescence in polystyrene is almost the same as that in frozen 2-MeTHF. The results of **1** and **2** were interpreted in terms that the T_1 state is in the local minimum geometry ($\mathbf{1T_{1b}}$ and $\mathbf{2T_{1b}}$), which is similar to the S_0-equilibrium geometry in frozen 2-MeTHF and polystyrene, as discussed in Section 3.3. On the other hand, there are no local minima in the T_1-PECs of **3** and **4**, as shown in Figure 4c,d. In such cases, it is likely that the geometry does not completely change to the T_1-global minimum geometry ($\mathbf{3T_{1a}}$ and $\mathbf{4T_{1a}}$) but moderately changes toward the T_1-global minimum in polystyrene. In other words, in polystyrene, the geometries of **3** and **4** are intermediate between the considerably distorted T_1-global minimum geometry and the slightly distorted T_1-geometry ($\mathbf{3T_{1b}}'$ and $\mathbf{4T_{1b}}'$) taken in the frozen 2-MeTHF. This is the reason why the energies of phosphorescence of **3** and **4** are lower in polystyrene than in frozen 2-MeTHF but higher than those in fluid 2-MeTHF. In addition, these results suggest that the rigidity of polystyrene is lower than that of frozen 2-MeTHF. The phosphorescence spectra of **3** and **4** in polystyrene are assigned as the π^*(dfppy) → dσ^*(Pt−Pt) transition because the Pt−Pt distance is shorter than 3.1 Å (see above).

4. Conclusions

Four kinds of 3,5-dialkylpyrazolate(R_2pz)-bridged platinum(II) dinuclear complexes, **1**−**4**, were theoretically investigated by the DFT(B3PW91) method to present detailed knowledge of their geometries and electronic structures in the T_1 state and to clarify the reason why the phosphorescence spectra significantly depend on the substituent on pz and the measurement conditions.

In **1** and **2** bearing H atoms and methyl groups on pz, respectively, the T_1-local minimum exists besides the T_1-global minimum. The Pt−Pt distance of the T_1-local minimum is similar to that of the S_0-equilibrium geometry, but the Pt−Pt distance of the T_1-global minimum is considerably shorter than that of the S_0-equilibrium one. The phosphorescence occurs at this local minimum in frozen 2-MeTHF at 77 K and polystyrene at RT because the geometry of the T_1 state is captured in this local minimum. This phosphorescence spectrum is assigned as the π^*(dfppy) → π(dfppy) + d(Pt) transition. In fluid 2-MeTHF at RT, the geometry of the T_1 state easily changes to the T_1-global minimum geometry ($\mathbf{1T_{1a}}$ and $\mathbf{2T_{1a}}$). Because geometries of $\mathbf{1T_{1a}}$ and $\mathbf{2T_{1a}}$ are much different from the S_0-equilibrium geometries, the energy of phosphorescence is much lower in fluid 2-MeTHF than in frozen 2-MeTHF and polystyrene. Because the T_1 state at the T_1-global minimum geometry is characterized as the ^{3}MMLCT excited state, the phosphorescence in fluid 2-MeTHF is assigned as the π^*(dfppy) → dσ^*(Pt−Pt) transition.

In **3** and **4** bearing methyl and/or *tert*-butyl substituents on pz, no local minimum is optimized in the T_1 state. The reason is easily understood as follows: Because the bulky *tert*-butyl substituents strongly push the dfppy plane away to decrease the Pt−Pt distance, the dσ^*(Pt−Pt) → π^*(dfppy) excited state becomes stable, and the π(dfppy) + d(Pt) → π^*(dfppy) excited state cannot become a local minimum. The geometry of the T_1 state changes slightly in frozen 2-MeTHF at 77 K except for the Pt−Pt distance, and it moderately changes in polystyrene at RT unlike in **1** and **2**. This is because the T_1-local minimum is absent in the T_1-PEC. Thus, the energy of phosphorescence is somewhat lower in polystyrene than in frozen 2-MeTHF. In fluid 2-MeTHF at RT, the geometry of the T_1 state completely changes to the T_1-global minimum geometry. This geometry change largely occurs in **3** but moderately in **4** because the Pt−Pt distance is already short in $\mathbf{4S_0}$ due to the presence of four *tert*-butyl groups on pz but still considerably long in $\mathbf{3S_0}$ due to the presence of two methyl groups. As a result, the energy of phosphorescence of **3** is much lower in fluid 2-MeTHF than in frozen 2-MeTHF, but that of **4** is moderately lower in fluid 2-MeTHF than in frozen 2-MeTHF. The phosphorescence spectra of **3** and **4** in these conditions are assigned as the π^*(dfppy) → dσ^*(Pt−Pt) transition.

In conclusion, interesting phosphorescence spectra of these pz-bridged dinuclear platinum(II) complexes are successfully understood in terms of their PECs of the T_1 state.

Acknowledgment. This work was financially supported by Grant-in-Aids on basic research (No. 15350012), Priority Areas for "Molecular Theory for Real Systems" (No. 461), NAREGI Project from the Ministry of Education, Science, Sports, and Culture, and Research Fellowship of the Japan Society for the Promotion of Science for Young Scientists. Some of the theoretical calculations were performed with SGI workstations of Institute for Molecular Science (Okazaki, Japan), and some of them were carried out with the PC cluster computers in our laboratory.

Supporting Information Available: Complete information for ref 16. S_0- and T_1-optimized geometries of **2** and **3** (Figure S1). Several important molecular orbitals of **2**, **3**, and **4** (Figure S2). This material is available free of charge via the Internet at http://pubs.acs.org.

IC702367F